01 Aug 2016

A Dissolution-Precipitation Mechanism is at the Origin of Concrete Creep in Moist Environments

Isabella Pignatelli

Aditya Kumar
Missouri University of Science and Technology, kumarad@mst.edu

R. Alizadeh

Yann Le Pape

et. al. For a complete list of authors, see https://scholarsmine.mst.edu/matsci_eng_facwork/1959

Recommended Citation

I. Pignatelli et al., "A Dissolution-Precipitation Mechanism is at the Origin of Concrete Creep in Moist Environments," *Journal of Chemical Physics*, vol. 145, no. 5, American Institute of Physics (AIP), Aug 2016.
The definitive version is available at https://doi.org/10.1063/1.4955429

A dissolution-precipitation mechanism is at the origin of concrete creep in moist environments

Isabella Pignatelli,[1] Aditya Kumar,[2] Rouhollah Alizadeh,[3] Yann Le Pape,[4] Mathieu Bauchy,[5,a)] and Gaurav Sant[1,6,a)]

[1]*Laboratory for the Chemistry of Construction Materials (LC^2), Department of Civil and Environmental Engineering, University of California, Los Angeles, California 90095, USA*
[2]*Materials Science and Engineering Department, Missouri University of Science and Technology, Rolla, Missouri 65409, USA*
[3]*Giatec Scientific, Ottawa, Ontario K2H 9C4, Canada*
[4]*Oak Ridge National Laboratory, Oak Ridge, Tennessee 37831, USA*
[5]*Physics of AmoRphous and Inorganic Solids Laboratory (PARISlab), Department of Civil and Environmental Engineering, University of California, Los Angeles, California 90095, USA*
[6]*California Nanosystems Institute (CNSI), University of California, Los Angeles, California 90095, USA*

(Received 21 March 2016; accepted 23 June 2016; published online 2 August 2016)

Long-term creep (i.e., deformation under sustained load) is a significant material response that needs to be accounted for in concrete structural design. However, the nature and origin of concrete creep remain poorly understood and controversial. Here, we propose that concrete creep at relative humidity ≥ 50%, but fixed moisture content (i.e., basic creep), arises from a dissolution-precipitation mechanism, active at nanoscale grain contacts, as has been extensively observed in a geological context, e.g., when rocks are exposed to sustained loads, in liquid-bearing environments. Based on micro-indentation and vertical scanning interferometry data and molecular dynamics simulations carried out on calcium–silicate–hydrate (C–S–H), the major binding phase in concrete, of different compositions, we show that creep rates are correlated with dissolution rates—an observation which suggests a dissolution-precipitation mechanism as being at the origin of concrete creep. C–S–H compositions featuring high resistance to dissolution, and, hence, creep are identified. Analyses of the atomic networks of such C–S–H compositions using topological constraint theory indicate that these compositions present limited relaxation modes on account of their optimally connected (i.e., constrained) atomic networks. *Published by AIP Publishing.* [http://dx.doi.org/10.1063/1.4955429]

I. INTRODUCTION

Second to water, concrete is by far the most widely used material in the world.[1] Due to the abundance of the necessary raw materials and the inexpensive nature of ordinary Portland cement (OPC), the binder used in concrete, this status is unlikely to change in the near future. However, cementitious materials undergo evolutions in structure and properties in time, resulting in volume change (i.e., shrinkage and creep), especially upon drying or due to imposed loads, which can ultimately result in fracture and failure.[2] Creep manifests as a time-dependent volume change under sustained load, which can cause dramatic deformations in the infrastructure.[3] However, the physical origin of creep in concrete remains poorly understood.[4] It is thought that the creep of concrete, particularly at later ages, is largely caused by the viscoelastic and viscoplastic nature of the calcium–silicate–hydrate (C–S–H),[5] the major binding phase in concrete, that is formed when cement (and cementitious compounds) reacts with water.[6] While secondary cementitious phases can show viscoelastic behavior,[7–9] the rate and extent of deformation of such phases are far less significant than those of the C–S–H.[5] As such, elucidating the mechanism of C–S–H creep is of primary importance in the context of predicting and limiting delayed deformations under load. Knowledge of such a mechanism would allow one to understand the relationship between creep and binder composition—a potential route to mitigate creep and better predict long-term engineering behavior.

Different models of C–S–H (cement paste, and concrete) creep have been proposed, although it is generally acknowledged that none of the existing models are able to explain all the experimental observations.[10] This suggests that the mechanism of creep may change in relation to environmental conditions (i.e., temperature, relative humidity (RH), and applied load) or that several creep mechanisms may operate simultaneously. Typical models that aim to describe creep in C–S–H suggest mechanisms based on (i) shear deformations of the C–S–H grains,[11] (ii) consolidation due to seepage and redistribution of pore water under stress,[12] (iii) rearrangements of the C–S–H gel due to the formation, followed by rupture of inter-granular bonds and their rearrangements (e.g., similar to the idea of displacive transitions in crystals) under relative motion,[13] (iv) rearrangements of C–S–H grains (under load) following a granular media analogy,[14] and/or (v) optimization of the alignment of the C–S–H layers.[5] Broadly, these models rely on the premise that the sliding action of the C–S–H grains

a)Authors to whom correspondence should be addressed. Electronic addresses: bauchy@ucla.edu and gsant@ucla.edu

or layers, with respect to each other enables a global structural reorganization.

While we do not contest the premise of structural reorganization (e.g., see Ref. 15), we propose an alternative origin and assess the hypothesis of a dissolution-precipitation mechanism as being at the origin of C–S–H creep in moist environments (RH ≥ 50%). This creep mechanism, well known in geology, contributes to upper-crustal deformations[16] and has been observed in aggregates of rock salt immersed in brine at room temperature.[17] The physical mechanism is proposed to involve the following steps:

(a) An applied external (mechanical) load induces local stresses between adjacent mineral (in this case, C–S–H) grains.
(b) This stress correspondingly provokes a change in the chemical potential of the solid.
(c) Following Le Chatelier's principle, the chemical equilibrium between the solid and liquid is shifted, which in turn enhances the solubility of the C–S–H in the liquid phase as a means of accommodating the applied stress.
(d) As the C–S–H dissolves, dissolved species diffuse through the water film to regions of lower ion activity (concentration) following Fickian diffusion.
(e) This series of events results in the formation of a precipitate, similar (if not equivalent) to the dissolved C–S–H phase, on the surfaces of unstressed C–S–H grains. This leads to the development of a plastic strain in order to accommodate the stress. This series of events persists as long as the applied stress exists.

Such a process has recently been reported to control creep in gypsum plaster[18] and has been suggested to also apply to hydrated cement solids.[18] According to this model, under appropriate (sufficient) moisture levels, creep would be a consequence of the dissolution of C–S–H in inter-granular water (i.e., pore solution that includes the capillary and gel water[15]) in high-stress regions. Based on an original approach combining micro-indentation studies of mechanical properties, vertical scanning interferometry (VSI) based analysis of aqueous dissolution rates of C–S–H, and molecular dynamics simulations of C–S–H of varying compositions, we identify a significant correlation between creep and dissolution, which supports a dissolution-precipitation mechanism being at the origin of concrete creep.

II. MATERIALS AND METHODS

A. C–S–H synthesis

C–S–H compositions were synthesized by mixing stoichiometric amounts of CaO and SiO_2 in water at room temperature. CaO was prepared from the calcination of $CaCO_3$ (Sigma-Aldrich) at 900 °C in a muffle furnace for 24 h. The CaO that is freshly obtained by this method is much more reactive than reagent-grade pure CaO. Amorphous SiO_2 (Cab-O-Sil, Grade M-5, Cabot Corporation) was dried at 80 °C over-night to remove surface adsorbed water. Distilled de-aired water was used for the aqueous solutions. A water (i.e., liquid) to solid (w/s, mass ratio) of 10 was used in each preparation. The CaO and SiO_2 were first dry-mixed and then shaken in high-density polyethylene (HDPE) bottles. Water was subsequently added to the mixture. Eventually, the bottles were sealed and additionally shaken. After the initial shaking, the plastic bottles were mounted on racks rotating at 16 rpm. Hydration was continued for 6 months to ensure equilibrium between the precipitated phase, i.e., C–S–H, and the contacting solution (solvent). It should be noted that variations in the Ca/Si molar ratio were achieved by adjusting the stoichiometric amounts of the reactants. Following the synthesis, the samples were filtered to remove the excess water. The gel-like material (surface-wet) was dried under vacuum for 3–4 days. During these steps, care was taken to avoid or minimize the exposure of the material to the atmosphere, i.e., to prevent carbonation. After drying, the C–S–H powders were stored in glass vials purged with nitrogen gas in a glove box until the time of use.

B. C–S–H characterization

C–S–H preparations obtained show well-defined X-ray patterns with three main peaks at about 1.250, 0.304, and 0.280 nm as reported in the literature[6] (see Figure 1). The XRD analysis showed slight traces of carbonate impurities in the final C–S–H powder only for Ca/Si = 1.5, 1.8. Expectedly, Ca/Si = 1.8 also shows portlandite contamination—as phase pure C–S–H free of (non-microcrystalline) portlandite cannot be obtained for Ca/Si > 1.55.[19] The thermogravimetric curves of C–S–H (i.e., mass loss and heat flow versus temperature) are qualitatively and quantitatively similar to those reported for C–S–H as reported in the literature.[6] A small mass loss in the region of 400-600 °C was noted for Ca/Si = 1.8, which contains portlandite (<2 mass %, N.B.: it is not possible to synthesize C–S–H for Ca/Si > 1.55 free of portlandite[19]) and in the region of 650-800 °C for Ca/Si = 1.5, 1.8, which contain calcium carbonate impurity (2-3 mass%) due to the contact of C–S–H with gaseous CO_2 over time. The average Ca/Si ratio for all C–S–H compositions was assessed by SEM-EDS analyses, nominal values (within ≤0.02 molar units) for which are noted in Figure 1. It should be noted however that the small quantities of impurities (≤5 mass %, for any given C–S–H composition) present are not expected to exert major influences on C–S–H behavior.

C. Micro-indentation

The C–S–H samples were conditioned to a uniform moisture state of 11% RH for several months, after which, they were used in micro-indentation analyses. In brief, the creep resistance of the C–S–H compositions was measured by applying a constant indentation load (P_{max} = 1.0 N) over a 600 s duration. In agreement with previous nano-indentation studies,[14] the penetration depth $\Delta h(t)$ increases logarithmically with time, fitted by the following equation:

$$\Delta h(t) = x_1 \log(1 + x_2 t) + x_3 t + x_4, \quad (1)$$

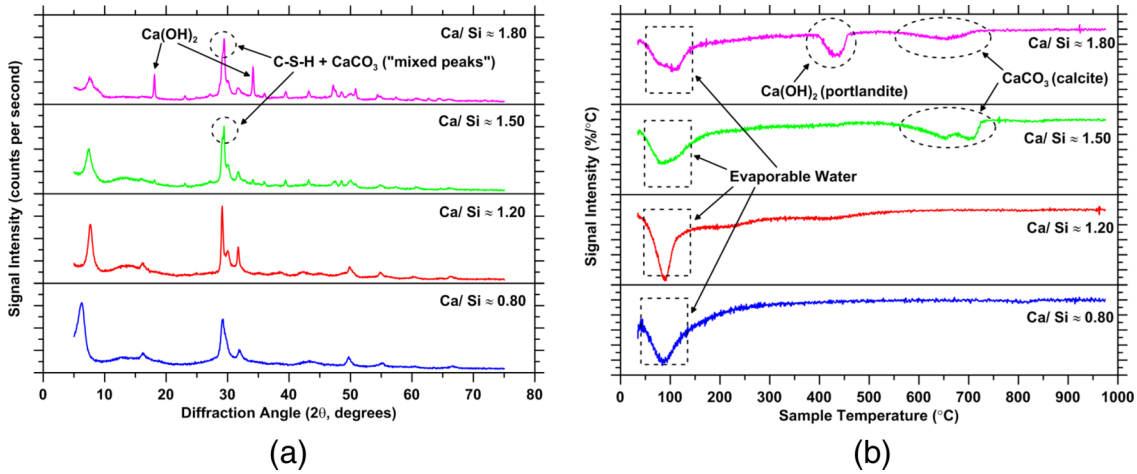

FIG. 1. (a) Representative x-ray reflections for the different C–S–H compositions. Duly marked are solid phases present as "impurities" in the C–S–H. (b) Differential mass loss (DTG) as a function of sample temperature for the different C–S–H compositions. Duly marked are solid phases present as "impurities" in the C–S–H.

where x_1, x_2, x_3, and x_4 are fitting parameters. The creep modulus C can be calculated as $C = P_{\max}/[2\left(\frac{A_c}{\pi}\right)^{\frac{1}{2}} x_1]$, where A_c is the projected area of contact between the indenter probe and the indenter surface.[20]

D. Vertical scanning interferometry

The dissolution rates of C–S–H particulates were quantified using vertical scanning interferometry[21] (VSI). VSI permits quantitative 3D-imaging of surfaces and interfaces, both in air and in liquids.[22,23] The technique allows the visualization of large areas (10 s of mm^2), with a lateral (X-Y) resolution of ≈500 nm and sub-nanometer resolution (≈0.1 nm) in the vertical, i.e., the Z-direction. These capabilities render VSI an optimal technique to visualize small changes in topographical profiles, driven by dissolution or precipitation at mineral surfaces and interfaces.[22,23] In typical dissolution studies, a volume of solvent (i.e., around 50-75 μl) contacts with the solute and ensures its dissolution. For the typical mass of solid used, this translates to a liquid-to-solid (l/s, mass basis) ratio in the range of 50 000–75 000 and approximates the dilute limit, and thus minimizes the potential for the (re-)precipitation of primary, or secondary phases. Our previous work[21] has quantified the typical uncertainty in the measured dissolution rates for inorganic minerals to be ±10%. A detailed explanation of the procedure is noted elsewhere.[21] Herein, buffer solutions were used to "fix" the pH of the solvent that induces dissolution. Due to the highly unsaturated conditions (i.e., with respect to the dissolving solute; C–S–H) and the high l/s, the pH of the solution is not expected to be affected by fractional dissolution of C–S–H over the course of the experiment.

E. Atomistic models of C–S–H

In the present work, we used the C–S–H model of Pellenq *et al.*[24,25] This structure of C–S–H, across a range of compositions (Ca/Si molar ratio), was obtained by introducing defects into an 11 Å tobermorite configuration in a combinatorial fashion.[26] The starting configuration of 11 Å tobermorite consists of pseudo-octahedral calcium oxide sheets, surrounded on each side by silicate chains. These negatively charged calcium–silicate layers are separated from each other by dissociated and undissociated interlayer water molecules and by charge-balancing calcium cations. Starting from this structure, the Ca/Si ratio is systematically increased from 1.0 to 2.0 by randomly removing [SiO_4] groups.[24] The introduced defects offer sites for the adsorption of extra water molecules, which was performed using the Grand Canonical Monte Carlo (GCMC) method—by equilibrating the defected structure with bulk water at constant volume and room temperature (100% RH). The ReaxFF interatomic potential[27,28] was then used to account for the reaction of the interlayer water with the defective calcium–silicate sheets. The use of a reactive potential permits the dissociation of water molecules into hydroxyl groups. The details of the methodology used for the preparation of the models as well as comparisons of computed properties to experimental data can be found elsewhere.[25] In this study, we retain the original ReaxFF potential,[27,28] with a timestep of 0.25 fs. The samples were relaxed to zero stress before further assessments were performed.

F. Topological constraints' enumeration through MD

Several issues complicate constraints' enumeration in silicate materials (see Section IV). In brief, (1) the coordination number (CN) of each species is not always known. Moreover, it has been shown that the effective number of bond stretching (BS) constraints created by each atom is not always equal to the CN (e.g., as calculated by enumerating the number of neighbors inside the first coordination shell). (2) Isolated atoms or molecules (e.g., water molecules[29]) are not part of the network and do not contribute to its rigidity. Therefore, they should not be taken into account in the constraints enumeration. (3) Each constraint is associated with a given energy and can, consequently, be intact or broken depending on the temperature, i.e., the amount of available thermal energy.[30–32] Thus, weaker angular constraints, like the Si–O–Ca angular bond in C–S–H, are broken at 300 K.[29]

Thus, one cannot rely on unproven guesses to enumerate the number of constraints.

Molecular dynamics (MD) simulations offer full access to the structure and dynamics of the atoms and provide a means for rigorous constraint enumeration. Towards this end, we have developed a general method that permits computation of the number of constraints in network glasses (e.g., see Refs. 33 and 34 for glasses and Refs. 29 and 35 for C–S–H). The method is based on the analysis of atomic trajectories obtained through MD simulations. Since the nature of the constraints imposed on atomic motions is not known *a priori*, we examine the motion of each atom and deduce the underlying constraints than cause this motion. The basic idea of this method is as follows: an active constraint would maintain bond lengths or angles fixed around their average values, whereas a large atomic motion (displacement) implies the absence of an underlying constraint. Therefore, to assess the number of BS constraints that apply to a central atom, we observe the radial excursion of each neighboring atom. If a neighbor shows a small radial excursion, then it implies the existence of an underlying constraint that maintains the bond length fixed around its average value. On the contrary, if the radial excursion is large, the corresponding constraint is broken. The limit between intact and broken constraints has been found to lie around a relative excursion of 7%,[29,30] which is fairly close to the Lindemann criterion.[36] We note, however, that the relative excursions of intact and broken constraints typically significantly differ from each other (see Ref. 29), so that the enumeration only weakly depends on the value of this threshold. The number of bond bending (BB) constraints can be accessed in the same fashion by analyzing the angular excursion of each neighbor. The detailed implementation of this method is reported elsewhere[29,30] and provides a means to clearly discriminate intact from broken constraints.

III. RESULTS

A. Creep propensity of C–S–H with respect to Ca/Si

In order to demonstrate or refute the hypothesis of a dissolution-precipitation mechanism controlling the creep of C–S–H, we studied, by experiments and simulations, the composition dependence of creep (Figure 2) and dissolution in C–S–H (Figure 3). Therefore, C–S–H's of different compositions ($0.8 \leq Ca/Si \leq 1.8$, molar ratio) were synthesized from the pozzolanic reaction between CaO and amorphous SiO_2 (see Section II). C–S–H solids with different packing fractions φ were prepared by compaction under pressure P (φ being a function of P), and their resistance to creep was examined by micro-indentation. As reported elsewhere,[9] we assume that the C–S–H compacts are representative of the C–S–H phase in hardened cement paste, i.e., showing similar elastic modulus, hardness, and creep modulus correlations as a function of their packing fraction. We focus on basic creep, that is, creep occurring without an accompanying change in the internal moisture state (content). During the indentation analysis, the relative humidity of pre-conditioned C–S–H samples remained fixed at 11% RH.

This low "conditioning" RH corresponds to the existence of a single monolayer of water (i.e., a statistical monolayer) on the C–S–H surfaces and the presence of the full amount of interlayer water inside the solid C–S–H.[15] For these RH conditions, it may be thought that significant dissolution of the C–S–H is unlikely to occur. However, recent atomistic simulation results have revealed that, for RH ≈ 7%, the interstitial space between two surfaces of C–S–H separated by 10 Å was almost fully occupied by adsorbed water molecules[37]—whose mobility would only increase with the pore width (and RH). This suggests that, although there is a single monolayer of water on the C–S–H surface on average,

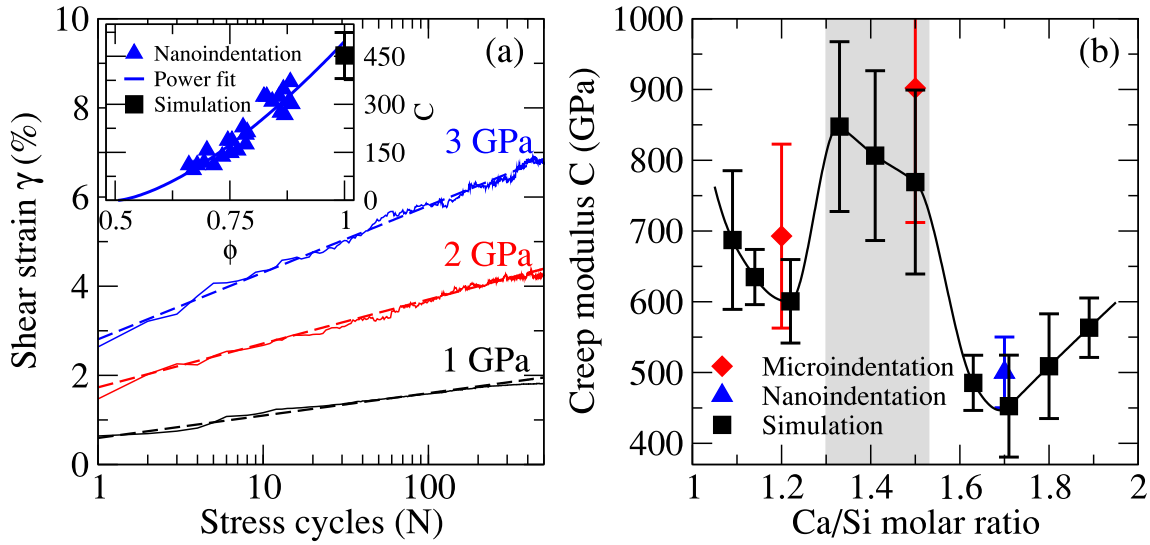

FIG. 2. Logarithmic creep of solid calcium–silicate–hydrate (C–S–H). (a) Shear strain γ of solid C–S–H (Ca/Si = 1.7) as a function of the number of applied stress perturbation cycles, when subjected to shear stresses (τ) of 1, 2, and 3 GPa. The dashed lines show logarithmic fits to $\gamma = (\tau/C)\log(1 + N/N_0)$, permitting evaluation of the creep modulus C. The inset shows C as a function of packing fraction φ, as obtained by nano-indentation.[14] The values are fitted by a power law expression $C = A\,(\varphi - 0.5)^{\alpha}$ and extrapolated to zero porosity to allow comparison to the simulation data. (b) The computed creep modulus of solid C–S–H as a function of the Ca/Si molar ratio (the values are taken from Ref. 38). The values are compared with experimental data obtained by micro-indentation[9] and nano-indentation.[14] The grey area indicates the compositional window in which the highest resistance to creep is observed.

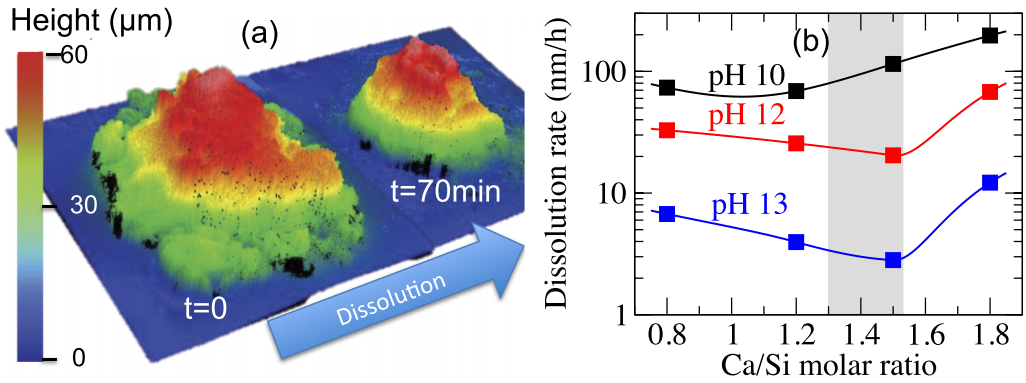

FIG. 3. Dissolution of calcium–silicate–hydrate (C–S–H). (a) Illustration of C–S–H (Ca/Si = 0.8, pH = 10) dissolution as visualized using vertical scanning interferometry (VSI) at zero time and after 70 min of solvent contact time. For each C–S–H particle, the horizontal resolution is 200×200 μm. Dissolution is tracked by measuring the decrease in the particle's height in time. (b) Dissolution rates (25 °C, 1 bar) of C–S–H samples as a function of Ca/Si at different pH. The grey band indicates the compositional window in which a maximum resistance to creep and dissolution is observed (see Figures 2 and 4).

the amount of water present between points of contact of adjacent C–S–H grains could be much larger; where stresses would be the largest and where dissolution is potentially most favored. While arguably, dissolution (and hence creep) would be significantly enhanced and favored when liquid water is present—creep is also influenced by composition-driven mechanical instability of the C–S–H phases as captured by rigidity theory (see Section IV). As discussed further below, this atomistic instability either favors or hinders the dissolution of a given C–S–H composition, vis-à-vis, others.

Micro-indentation creep tests carried out on C–S–H compacts show that, under a constant indentation load, a continuous increase of the penetration depth is observed (see Ref. 9 for more details), which, in agreement with previous nano-indentation experiments,[14] suggests that the creep of C–S–H is logarithmic with the time. Following a well-established methodology,[9] the indentation hardness H, indentation modulus M, and creep modulus C were quantified. These quantities depend on the packing fraction ϕ, which was determined using helium pycnometry.[14] In order to evaluate the dependence of C on the composition (i.e., Ca/Si molar ratio) of C–S–H without any contribution from the porosity, the results were extrapolated to zero porosity (i.e., "solid C–S–H"). However, due to the lack of accuracy in assessing φ precisely, direct extrapolation is challenging.

Nevertheless, for a given C–S–H composition, C features a strongly linear correlation with H. The zero-porosity hardness H_0 of C–S–H samples of varying Ca/Si molar ratios was recently calculated by atomistic simulations and shown to be in excellent agreement with experimental data.[25,39] As such, by fitting C versus H and extrapolating C to $H = H_0$, one can estimate the creep modulus at zero porosity, as shown in Figure 2(b), along with data obtained via nano-indentation for Ca/Si = 1.7.[14] We note that C–S–H with Ca/Si = 1.5 exhibits the highest resistance to creep, with a creep modulus around 80% higher than that obtained for Ca/Si = 1.7. Such non-linear behavior is very different from that of indentation hardness and creep modulus, both of which decrease monotonically with Ca/Si.[25] The details of the indentation study and the presentations of $C(H)$ linear curves that permit extrapolation of C to zero porosity can be found elsewhere.[9]

B. Molecular dynamics simulations of C–S–H creep

To obtain detailed insights into the physical mechanism of creep in C–S–H, molecular dynamics (MD) simulations were carried out. The atomistic model of C–S–H of Pellenq *et al.*[24,25] was used as an initial starting point of the calculations. The model of Pellenq *et al.*,[24,25] while contentious, has been noted to accurately recover the mechanical properties (i.e., indentation modulus and hardness) of C–S–H in excellent agreement with experimental data.[25] While we admit that the model is imperfect,[40–42] to the best of our knowledge, it offers the only means to "computationally assess" C–S–H compositions across a wide range of Ca/Si ratios. It should also be noted that the outcomes of this study—as noted below—are generic and do not rely strongly on the chosen C–S–H model. Although MD simulations are typically limited to a few nanoseconds, for this study, we developed a novel technique that allows the simulation of creep over longer timescales. This technique involves applying a constant shear stress τ, mimicking experimental measurements of deviatoric creep.[43] In addition to τ, small periodic stress perturbations[38,44] are applied in cycles (see Section II). Each perturbation cycle slightly deforms the energy landscape experienced by the system, thereby permitting jumps over select energy barriers, allowing the system to relax towards lower energy states.

Careful analysis of the internal energy shows that the height of the energy barriers, through which the system transits across each cycle, remains roughly constant over successive cycles. On the basis of transition state theory, which states that the time needed for a system to jump over an energy barrier E_A is proportional to $\exp(-E_A/kT)$, we can assume that each cycle corresponds to a constant duration Δt, so that a fictitious time can be defined as $t = N\Delta t$, where N is the number of cycles.[45] It should be noted that these transitions occur spontaneously, although the duration Δt before each jump is too long to be accessible from conventional atomistic simulations. We recently applied a similar accelerated relaxation method to

study room-temperature relaxation of silicate glasses[46] and showed that the dynamics of the relaxation do not depend on the amplitude of the stress perturbations, as long as they remain significantly lower than the yield stress of the material (N.B.: the yield stress of solid C–S–H across all compositions is >4 GPa). Figure 2(a) shows the computed shear strain γ of C–S–H with Ca/Si = 1.7 as a function of the number of stress perturbation cycles N, for different constant stresses τ = 1, 2, and 3 GPa. In agreement with experimental indentation profiles, we observe a logarithmic creep response, which can be written as

$$\gamma(N) = (\tau/C)\log(1 + N/N_0), \quad (2)$$

where N_0 is a fitting parameter and C is the creep modulus (i.e., the inverse compliance, GPa) which is determined by fitting the computed shear strain-stress cycle plot (see Figure 2(a)). Interestingly, we find that the computed shear strains are proportional to the applied constant shear stress τ. As such, C does not depend on the applied stress and, thereby, emerges as an intrinsic property of the material. We note however that this is true only so long as the applied stress is lower than the yield stress of the sample.[44] Further, since the simulations do not consider any porosity, the computed values of C can only be compared to experimental values extrapolated to zero porosity. As shown in the inset of Figure 2(a), the obtained C (≈450 GPa) is in very good agreement with nano-indentation data (see Figure 2(b)),[14] extrapolated to a packing fraction of 1 (i.e., solid C–S–H, which does not contain any pores). Note that, in Ref. 14, the packing density was determined through micromechanics-based scaling relations. To the best of our knowledge, this is the first time that the creep propensity (i.e., as indicated by the creep modulus) of cementitious or other viscoelastic materials has been successfully reproduced by atomistic simulation. This approach was also applied to other C–S–H compositions to better understand the relationship between their composition and resistance to creep. As shown in Figure 1(b), the computed C values show a non-linear evolution with the Ca/Si, which manifests in the form of a broad maximum around Ca/Si = 1.5. Once again, the obtained C values are in excellent agreement with micro-indentation data extrapolated to zero porosity (Figure 2(b)).

C. Dissolution sensitivity of C–S–H with respect to Ca/Si

We now investigate whether a dissolution-precipitation sensitivity of creep, as a function of composition, would explain the maximum resistance to creep observed around Ca/Si = 1.5. In the dissolution-precipitation model, critical variables include the structure of the inter-grain contacts, grain packing and their size distributions, and identifying the slowest (i.e., rate controlling) step of the process. Due to the small spacing between inter-granular contacts (on the order of nanometers[37]), the transport of solubilized ions between grains will be fast under conditions of sufficient moisture and where transport confinement is slight, suggesting that the dissolution rate (i.e., rather than ionic diffusion) is rate-controlling. According to Raj's model,[17] the (creep) strain rate should be proportional to (1) the applied stress and (2) the dissolution rate and (3) inversely proportional to the grain size—although given the similar nanoscale dimension of C–S–H grains,[47] size is potentially less relevant. Since the effects of applied stress have already been examined in Sec. III B, we evaluated the kinetics of dissolution of C–S–H to examine its validity and relevance to creep behaviors.

The dissolution rates of C–S–H particulates (equivalent to those that formed the compacts used in micro-indentation analyses) with Ca/Si = 0.8, 1.2, 1.5, and 1.8 were measured using vertical scanning interferometry[21] (VSI, see Section II). The VSI technique has been extensively applied to measure the dissolution rates of minerals of geological and technological relevance.[48,49] By tracking the evolution of the surface topography in time, with sub-nanometer vertical resolution, VSI accesses the "true" dissolution rate of a dissolving solid. Unlike dissolution assessments that are based on analysis of solution compositions, which may be affected by aspects including metastable barrier formation, incongruency in phase dissolution, and/or ion adsorption, VSI analytics are not influenced by such complexities. Dissolution rates of the C–S–H solids were quantified using a rain-drop procedure,[21] wherein both the solution pH and composition (i.e., the under-saturation level with respect to the dissolving solid) are kept constant over the course of the experiment (see Figure 3(a)). Dissolution experiments were conducted at room temperature and at pH 10, 12, and 13, the latter value corresponding to the pH of the pore-fluid in mature cement pastes.[47]

Figure 3(b) shows the dissolution rates of the various C–S–H compositions as a function of the Ca/Si molar ratio, for different solvent pH's. The dissolution rates, broadly, show order of magnitude agreement with other quantifications of C–S–H dissolution rates noted in the literature.[50–55] It should be clarified, however, that such agreement emerges only when dissolution rates measured by analyses of solution compositions (e.g., using ICP-OES: inductively coupled plasma optical emission spectrometry) are rescaled by a factor $R = [S/V]_T/[S/V]_E$—such that $r_{VSI} = R{\cdot}r_{solution}$, where S is the specific surface area of the solid per unit mass (including internal pore surface if any), V is the volume of the solid per unit mass, the subscripts T and E denote the total and external contributions to surface area (i.e., for a non-porous solid, $[S/V]_T = [S/V]_E$), r is the dissolution rate (written in units of mol/m^2 s), and the subscripts VSI and solution denote dissolution rates estimated by VSI analyses or analyses of solution concentrations, respectively. As a point of reference, without rescaling, C–S–H dissolution rates measured by VSI differ from those analyzed by analysis of solution concentration by around 3–5 orders of magnitude.

Such rescaling needs to be carried out because when phase dissolution is measured via solution phase analysis, the dissolution rate is obtained by multiplying the concentration difference (of ions) in the input and output streams (e.g., see Refs. 50 and 53) by a constant written as $[q/(A\nu)]$, where q is the volumetric flux, A is the specific surface area of the dissolving solid, and ν is a coefficient that enforces a particular stoichiometry to an (assumed) dissolution reaction. This approach assumes that the entire surface accessible to the probe vapor, e.g., N_2, often used in specific

surface area analyses is equally susceptible to dissolution. While this assumption is imperfect, but acceptable at a first approximation for solids which present modest internal surface area,[48,56,57] this assumption is inappropriate for highly porous precipitates such as C–S–H which feature significant small (micro-/meso-scale) pores—within which dissolution as estimated by a "flux" is negligible, if any. For a solid such as C–S–H which shows a specific surface area on the order of 100 m^2/g,[58,59] this nature of normalization tends to artificially suppress the dissolution rate.

On the other hand, assessments of dissolution rates using vertical scanning interferometry are arrived at by measuring the change in height of a dissolving surface as a function of time. The change in height reported represents an "areal average" wherein the height over a given region (e.g., over the contours of a particle which are sampled at a lateral resolution of 500 nm in the X-Y coordinates and around 0.1 nm in the Z-coordinate) is measured and averaged. As a result, the dissolution rate is presented as an area averaged surface retreat velocity with units of nm/h. In such measurements, the area participating in dissolution is that which is "exposed or visible" to the VSI objective. Thus, no assumption is made on the participation (or lack thereof) of the occluded internal surface area in dissolution. While this approach is reasonable for slightly porous materials wherein "in-pore dissolution is negligible," it may "artificially enhance" the dissolution rate under conditions where significant in-pore dissolution occurs. In summary, it is fair to estimate that the true dissolution rate of a complex, porous solid, such as C–S–H, lies in between the quantifications of VSI and solution phase techniques. In addition to these inconsistencies in the surface area, C–S–H is also sensitive to the methods of its synthesis and aging, parameters which influence both its structure and dissolution rate.

Coming back to trends in C–S–H dissolution rates (Figure 3(b)), we note that, for every C–S–H composition, the dissolution rate decreases with pH, as also observed for limestone, alite, ordinary Portland cement (OPC), and gypsum—since the under-saturation level, described to the first order by the hydroxyl ion activity, decreases (i.e., becoming a smaller number, with a negative sign) accordingly.[21] In addition, at constant pH, we observe a strongly non-linear evolution of the dissolution rate as a function of Ca/Si. Interestingly, at pH's of 12 and 13, a dissolution minimum is observed for Ca/Si = 1.5, that is, the range of compositions featuring an increased resistance to creep (see Figure 2(b) and related discussion). This minimum shifts to a lower Ca/Si at pH 10. This is a significant observation, which, as shown in the inset of Figure 4(a), indicates a strong correlation between dissolution and creep propensity, an observation which supports the hypothesis of a dissolution-precipitation mechanism as being at the origin of concrete creep in moist environments. It should be noted the qualifier "moist" suggests pores that contain water with bulk or *bulk-like* properties including pores exposed to the atmosphere and/or ink-bottle/dead-end pores—wherein bulk water may

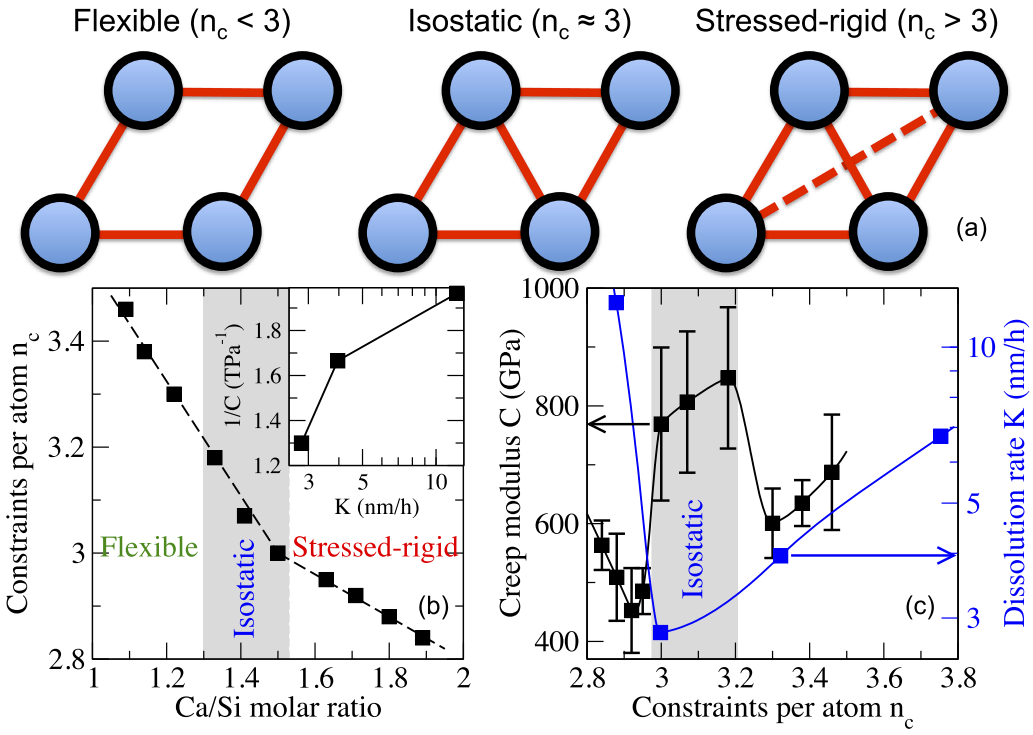

FIG. 4. Topological analysis of calcium–silicate–hydrate (C–S–H). (a) The three states of rigidity of a mechanical truss. Flexible networks feature internal degrees of freedom, and stressed-rigid ones show eigenstresses, whereas isostatic ones are rigid but free of internal stress. The dashed line indicates a frustrated constraint, which cannot be satisfied due to redundant constraints, thereby resulting in eigenstresses. (b) The number of topological constraints per atom (n_c) in C–S–H as a function of Ca/Si. The grey area indicates the compositional window in which maximum resistance to creep and dissolution is observed (see Figures 1 and 2), also corresponding to the range of isostatic compositions ($n_c \approx 3$), effectively separating the flexible ($n_c < 3$) from the stressed-rigid domains ($n_c > 3$). The inset shows the correlation between the inverse of the creep modulus C and the dissolution rate of C–S–H. (c) The creep modulus C and dissolution rate of C–S–H at pH = 13 as a function of n_c (the creep values are taken from Ref. 38). The grey area indicates the isostatic C–S–H compositions.

remain shielded by smaller pore entryways and would hence not deplete until lower RHs.[15]

IV. DISCUSSION

Based on the atomistic simulations detailed above, we aim to identify and rationalize the *common structural origin* of the maximum in resistance to creep and dissolution observed around Ca/Si = 1.5. To this end, we applied topological constraint theory (TCT),[60–62] a framework which has been successfully applied to understand compositional controls on the properties of glasses.[35,63,64] TCT captures the topology of atomic networks while filtering out less relevant structural details that ultimately do not affect the macroscopic response. Within the TCT framework, atomic networks are described as mechanical trusses, in which the atoms experience displacement constraints, as imposed by the radial and angular chemical bonds. Therefore, following Maxwell's stability criterion,[65] an atomic network is described as flexible, stressed-rigid, or isostatic, if the number of topological constraints per atom (n_c) is lower, higher, or equal to three, i.e., the number of degrees of freedom per atom in three dimensions (see Figure 4(a)).

Our use of TCT is stimulated by the observation that isostatic glasses tend to show weak aging over time,[66,67] a feature potentially relevant to C–S–H and hence concrete creep. Recently, we extended TCT to handle poorly crystalline materials like C–S–H.[29] Interestingly, as shown in Figure 4(b), we note that C–S–H features a rigidity transition at Ca/Si = 1.5,[35] while being stressed-rigid ($n_c > 3$) at low Ca/Si and flexible ($n_c < 3$) at higher Ca/Si. As such, as shown in Figure 4(c), we observe that a maximum resistance to creep and dissolution is achieved when the atomic network is isostatic ($n_c = 3$) at Ca/Si = 1.5. This constitutes, to the best of our knowledge, the first quantitative evidence of a link between the atomic network topology (and hence composition) and resistance to creep and dissolution.

To explain these results, we propose the following atomistic view. (1) Due to a lack of mechanical constraints, flexible atomic networks feature internal floppy modes of deformation.[61] These low-energy modes facilitate the reorganization of the network under stress (for example, see recent experimental evidence for the reorganization of C–S–H in cement paste, under the imposition of a hydrostatic drying stress[15]), thereby enhancing creep. Similarly, lower network connectivity ($n_c < 3$) has been shown to enhance dissolution.[68] (2) On the other hand, stressed-rigid atomic networks show internal eigenstresses,[69] which originate from a steric frustration of the network. Indeed, due to their high number of chemical bonds, some constraints in stressed-rigid networks become redundant, that is, all of them cannot be satisfied simultaneously—just as it would be impossible to adjust one of the angles of a rigid triangle with three edges fixed. These internal stresses induce instabilities in the network and, thereby, act as a driving force for phase separation or devitrification of glasses.[62,70] Such an instability, represented by an increase in entropy, also enhances dissolution sensitivity. It should be noted that such instabilities will only be observed in disordered materials, as pristine crystals, on account of their optimized geometry, have a structure that does not induce any internal stress—in absence of an external stimulus. In others words, even if the number of topological constraints inside a crystal becomes larger than the number of degrees of freedom, all the constraints remain compatible with each other, so that no internal frustration is created.

Coming back to creep, stressed-rigid glasses have been noted to display slight elastic recovery after pressurization (densification).[71] Indeed, once placed under pressure, due to their high number of constraints, their network remains permanently locked in its densified state.[72] If creep is seen as a succession of small cycles as stress, in stressed-rigid C–S–H compositions, each cycle will induce an irreversible deformation (i.e., compaction in the case of compression and elongation in the case of tensile loading), thereby resulting in significant accumulative deformations with longer imposed stress durations and, as a result, lower resistance to creep.

Alternatively, these results can be understood by considering the roughness of the energy landscape, which is determined by both the bond and the floppy mode densities.[73] Indeed, the bond density, that is, their connectivity, tends to induce the creation of energy basins. In parallel, the floppy mode density leads to the formation of channels between these basins, therefore extending the possibilities of relaxation for the flexible networks, which enhances creep and dissolution. However, in stressed-rigid networks, the frustration created due to unsatisfied constraints acts as an elastic energy,[74] which, in turn, induces some jumps between the basins, which, again, extends the possibilities of relaxation. As such, isostatic networks do not feature any barrier-less channels between the basins and do not possess any eigenstress induced driving forces to jump over the energy barriers. Such optimally constrained networks therefore show limited modes of relaxation, which renders them resistant to creep and stable with respect to dissolution.

Finally, we note that our simulation results suggest the existence of two distinct transitions at Ca/Si = 1.3 and 1.5 (see Figs. 2(b) and 4(c)), although the limited number of experimental samples considered herein prevents us from firmly confirming this feature. Nevertheless, we note that, in network glasses, the flexible-to-rigid and unstressed-to-stressed transitions are indeed distinct from each other, in agreement with the present results. These two transitions effectively define the extent of the so-called Boolchand intermediate phase, in which atomic networks are rigid but free of eigenstress.[75,76] Interestingly, glasses belonging to this phase have been noted to show weak physical aging over time,[66,67] a feature that could be connected to the strong resistance to creep deformations observed herein. Altogether, these results suggest that optimally isostatic atomic networks tend to show optimal stabilities over time.

V. CONCLUSIONS

By simultaneously quantifying the propensity of C–S–H compositions to dissolve and to creep, we have clarified that dissolution and creep are strongly correlated with and indicative of each other. Such correlation offers the first direct

evidence, experimental and computational, that a dissolution-precipitation mechanism could be the origin of the concrete creep in moist environments—as has long been known for geological materials. More generally, we have shown that atomic topology is a fundamental variable that renders a material, sensitive or not, to aging and dissolution. This is significant as it provokes an opportunity for tuning material compositions. Thus, we find that shifting the composition of the binding C–S–H phase to lower Ca/Si (i.e., Ca/Si ≈ 1.5) would increase the resistance of concretes to both creep and dissolution.

It should be noted however that these conclusions only refer to C–S–H compositions whose moisture content is fixed (i.e., wherein no drying occurs). However, even in the case where the moisture content remains fixed, the imposition of a stress would result in (i) an internal redistribution of moisture and (ii) a change in the internal stress state, to favor dissolution and creep—as a means to relax the stress as the body creeps.[77] Depending on how this occurs, as moisture distributes internally, dissolution/precipitation (and hence creep) could increase in moisture rich zones, which can support more dissolution, and decrease in drier regions. On the other hand, since creep induces stress relaxations, the influence of stress on C–S–H dissolution would lift locally, following creep—resulting in reduced dissolution. Effects of this nature could result in spatial variations in creep—until the dominant process ensures that globally creep kinetics are altered. Actions of this nature when combined with the effects of drying (i.e., mass change, resulting in drying creep) and mechanical loading may explain the rate of creep deformations seen in practice and explain behaviors such as the Pickett effect that is seen in cementing systems[78–80] and have yet not been fully explained.

ACKNOWLEDGMENTS

The authors acknowledge full financial support for this research provided by the U.S. Department of Transportation (U.S. DOT) through the Federal Highway Administration (Grant No. DTFH61-13-H-00011), the National Science Foundation (Grant No. 1562066 and CAREER Award No. 1235269), the Oak Ridge National Laboratory operated for the U.S. Department of Energy by UT-Battelle (LDRD Award No. 4000132990), and the University of California, Los Angeles (UCLA). Access to computational resources was provisioned by the Physics of AmoRphous and Inorganic Solids Laboratory (PARISlab), the Laboratory for the Chemistry of Construction Materials (LC^2), and the Institute for Digital Research and Education (IDRE) at UCLA. This research was conducted in the Laboratory for the Chemistry of Construction Materials (LC^2) and Physics of AmoRphous and Inorganic Solids Laboratory (PARISlab) at UCLA. The authors gratefully acknowledge the support that has made these laboratories and their operations possible. The contents of this paper reflect the views and opinions of the authors, who are responsible for the accuracy of the datasets presented herein, and do not reflect the views and/or policies of the funding agencies nor do the contents constitute a specification, standard or regulation. This manuscript has been co-authored by the Oak Ridge National Laboratory, managed by UT-Battelle LLC under Contract No. DE-AC05-00OR22725 with the U.S. Department of Energy. The publisher, by accepting the article for publication, acknowledges that the U.S. Government retains a nonexclusive, paid-up, irrevocable, worldwide license to publish or reproduce the published form of this manuscript or allow others to do so, for U.S. Government purposes. The Department of Energy will provide public access to these results of federally sponsored research in accordance with the DOE Public Access Plan (http://energy.gov/downloads/doe-public-access-plan).

[1]K. Scrivener and H. Van Damme, MRS Bull. **29**, 308 (2004).
[2]Z. P. Bažant, Nucl. Eng. Des. **203**, 27 (2001).
[3]Z. Bažant, M. Hubler, R. Wendner, and Q. Yu, *Mechanics and Physics of Creep, Shrinkage, and Durability of Concrete* (American Society of Civil Engineers, 2013), pp. 1–17.
[4]Q. Zhang, "Creep properties of cementitious materials: Effect of water and microstructure: An approach by microindentation," Ph.D. thesis, Université Paris-Est, 2014.
[5]P. Acker, Mater. Struct. **37**, 237 (2004).
[6]H. F. W. Taylor, *Cement Chemistry* (Thomas Telford, 1997).
[7]J. J. Beaudoin, B. T. Tamtsia, and J. Marchand, Adv. Cem. Res. **14**, 135 (2002).
[8]V. S. Ramachandran and R. F. Feldman, J. Appl. Chem. **17**, 328 (1967).
[9]D.-T. Nguyen, R. Alizadeh, J. J. Beaudoin, P. Pourbeik, and L. Raki, Cem. Concr. Compos. **48**, 118 (2014).
[10]D.-T. Nguyen, "Microindentation creep of calcium-silicate-hydrate and secondary hydrated cement systems," Doctoral thesis, University of Ottawa, 2014.
[11]F. Thomas, in *International Association of Testing Materials, London Congress* (1937), pp. 292–294.
[12]C. G. Lynam, *Growth and Movement in Portland Cement Concrete* (London, 1934).
[13]H. M. Jennings, Mater. Struct. **37**, 59 (2004).
[14]M. Vandamme and F.-J. Ulm, Proc. Natl. Acad. Sci. U. S. A. **106**, 10552 (2009).
[15]H. M. Jennings, A. Kumar, and G. Sant, Cem. Concr. Res. **76**, 27 (2015).
[16]D. Dysthe, Y. Podladchikov, F. Renard, J. Feder, and B. Jamtveit, Phys. Rev. Lett. **89**, 246102 (2002).
[17]R. Raj, J. Geophys. Res. **87**, 4731, doi:10.1029/JB087iB06p04731 (1982).
[18]E. A. Pachon-Rodriguez, E. Guillon, G. Houvenaghel, and J. Colombani, Cem. Concr. Res. **63**, 67 (2014).
[19]B. Lothenbach and F. Winnefeld, Cem. Concr. Res. **36**, 209 (2006).
[20]W. C. Oliver and G. M. Pharr, J. Mater. Res. **7**, 1564 (1992).
[21]A. Kumar, J. Reed, and G. Sant, J. Am. Ceram. Soc. **96**, 2766 (2013).
[22]I. Koyuncu, J. Brant, A. Lüttge, and M. R. Wiesner, J. Membr. Sci. **278**, 410 (2006).
[23]O. V. Lyulko, G. Randers-Pehrson, and D. J. Brenner, Rev. Sci. Instrum. **84**, 053701 (2013).
[24]R. J.-M. Pellenq, A. Kushima, R. Shahsavari, K. J. V. Vliet, M. J. Buehler, S. Yip, and F.-J. Ulm, Proc. Natl. Acad. Sci. U. S. A. **106**, 16102 (2009).
[25]M. J. Abdolhosseini Qomi, K. J. Krakowiak, M. Bauchy, K. L. Stewart, R. Shahsavari, D. Jagannathan, D. B. Brommer, A. Baronnet, M. J. Buehler, S. Yip, F.-J. Ulm, K. J. Van Vliet, and R. J.-M. Pellenq, Nat. Commun. **5**, 4960 (2014).
[26]S. A. Hamid, Z. Kristallogr. **154**, 189 (1981).
[27]H. Manzano, S. Moeini, F. Marinelli, A. C. T. van Duin, F.-J. Ulm, and R. J.-M. Pellenq, J. Am. Chem. Soc. **134**, 2208 (2012).
[28]M. J. Abdolhosseini Qomi, M. Bauchy, F.-J. Ulm, and R. J.-M. Pellenq, J. Chem. Phys. **140**, 054515 (2014).
[29]M. Bauchy, M. J. Abdolhosseini Qomi, C. Bichara, F.-J. Ulm, and R. J.-M. Pellenq, J. Phys. Chem. C **118**, 12485 (2014).
[30]M. Bauchy and M. Micoulaut, J. Non-Cryst. Solids **357**, 2530 (2011).
[31]P. K. Gupta and J. C. Mauro, J. Chem. Phys. **130**, 094503 (2009).
[32]J. C. Mauro, P. K. Gupta, and R. J. Loucks, J. Chem. Phys. **130**, 234503 (2009).
[33]M. Bauchy, M. Micoulaut, M. Celino, S. Le Roux, M. Boero, and C. Massobrio, Phys. Rev. B **84**, 054201 (2011).
[34]M. Bauchy, Am. Ceram. Soc. Bull. **91**, 34 (2012).
[35]M. Bauchy, M. J. A. Qomi, C. Bichara, F.-J. Ulm, and R. J.-M. Pellenq, Phys. Rev. Lett. **114**, 125502 (2015).

[36]F. A. Lindemann, Phys. Z. **11**, 609 (1910).
[37]P. A. Bonnaud, Q. Ji, B. Coasne, R. J.-M. Pellenq, and K. J. Van Vliet, Langmuir **28**, 11422 (2012).
[38]M. Bauchy, M. Wang, Y. Yu, B. Wang, N. M. A. Krishnan, F.-J. Ulm, and R. Pellenq, e-print arXiv:1605.05043 [cond-mat] (2016).
[39]K. Ioannidou, K. J. Krakowiak, M. Bauchy, C. G. Hoover, E. Masoero, S. Yip, F.-J. Ulm, P. Levitz, R. J.-M. Pellenq, and E. D. Gado, Proc. Natl. Acad. Sci. U. S. A. **113**, 2029 (2016).
[40]K. L. Scrivener, P. Juilland, and P. J. M. Monteiro, Cem. Concr. Res. **78**, 38 (2015).
[41]G. Kovacevic, B. Persson, L. Nicoleau, A. Nonat, and V. Veryazov, Cem. Concr. Res. **67**, 197 (2015).
[42]I. G. Richardson, Acta Crystallogr. Sect. B: Struct. Sci., Cryst. Eng. Mater. **69**, 150 (2013).
[43]W. Vichit-Vadakan and G. W. Scherer, Cem. Concr. Res. **33**, 1925 (2003).
[44]M. Bauchy, E. Masoero, F.-J. Ulm, and R. Pellenq, "Creep of bulk C–S–H: Insights from molecular dynamics simulations," CONCREEP **10**, 511–516 (2015).
[45]E. Masoero, H. Manzano, E. Del Gado, R. J. M. Pellenq, F. J. Ulm, and S. Yip, *Mechanics and Physics of Creep, Shrinkage, and Durability of Concrete: A Tribute to Zdenk P. Bazant* (ASCE Publications, 2013), p. 166.
[46]Y. Yu, M. Wang, D. Zhang, B. Wang, G. Sant, and M. Bauchy, Phys. Rev. Lett. **115**, 165901 (2015).
[47]A. J. Allen, J. J. Thomas, and H. M. Jennings, Nat. Mater. **6**, 311 (2007).
[48]A. C. Lasaga and A. Luttge, Science **291**, 2400 (2001).
[49]P. M. Dove, N. Han, and J. J. D. Yoreo, Proc. Natl. Acad. Sci. U. S. A. **102**, 15357 (2005).
[50]N. C. Marty, S. Grangeon, F. Warmont, and C. Lerouge, Mineral. Mag. **79**, 437 (2015).
[51]J. R. Houston, R. S. Maxwell, and S. A. Carroll, Geochem. Trans. **10**, 1 (2009).
[52]I. Baur, P. Keller, D. Mavrocordatos, B. Wehrli, and C. A. Johnson, Cem. Concr. Res. **34**, 341 (2004).
[53]A. Trapote-Barreira, J. Cama, and J. M. Soler, Phys. Chem. Earth, Parts A/B/C **70**, 17 (2014).
[54]G. M. N. Baston, A. P. Clacher, T. G. Heath, F. M. I. Hunter, V. Smith, and S. W. Swanton, Mineral. Mag. **76**, 3045 (2012).
[55]P. Vieillard and F. Rassineux, Appl. Geochem. **7**, 125 (1992).
[56]A. Luttge and R. S. Arvidson, J. Am. Ceram. Soc. **93**, 3519 (2010).
[57]R. S. Arvidson and A. Luttge, Chem. Geol. **269**, 79 (2010).
[58]V. Baroghel-Bouny, Cem. Concr. Res. **37**, 414 (2007).
[59]A. Kumar, S. Ketel, K. Vance, T. Oey, N. Neithalath, and G. Sant, Transp. Porous Media **103**, 69 (2014).
[60]J. C. Phillips, J. Non-Cryst. Solids **34**, 153 (1979).
[61]M. F. Thorpe, J. Non-Cryst. Solids **57**, 355 (1983).
[62]J. C. Mauro, Am. Ceram. Soc. Bull. **90**, 31 (2011).
[63]M. M. Smedskjaer, J. C. Mauro, and Y. Yue, Phys. Rev. Lett. **105**, 115503 (2010).
[64]M. M. Smedskjaer, J. C. Mauro, S. Sen, and Y. Yue, Chem. Mater. **22**, 5358 (2010).
[65]J. C. Maxwell, Philos. Mag. Ser. **4**(27), 294 (1864).
[66]S. Chakravarty, D. G. Georgiev, P. Boolchand, and M. Micoulaut, J. Phys.: Condens. Matter **17**, L1 (2005).
[67]P. Chen, P. Boolchand, and D. G. Georgiev, J. Phys.: Condens. Matter **22**, 065104 (2010).
[68]A. Pelmenschikov, H. Strandh, L. G. M. Pettersson, and J. Leszczynski, J. Phys. Chem. B **104**, 5779 (2000).
[69]F. Wang, S. Mamedov, P. Boolchand, B. Goodman, and M. Chandrasekhar, Phys. Rev. B **71**, 174201 (2005).
[70]M. Micoulaut, Am. Mineral. **93**, 1732 (2008).
[71]A. K. Varshneya and D. J. Mauro, J. Non-Cryst. Solids **353**, 1291 (2007).
[72]J. C. Mauro and A. K. Varshneya, J. Am. Ceram. Soc. **90**, 192 (2007).
[73]M. Bauchy and M. Micoulaut, Nat. Commun. **6**, 6398 (2015).
[74]Y. Vaills, T. Qu, M. Micoulaut, F. Chaimbault, and P. Boolchand, J. Phys.: Condens. Matter **17**, 4889 (2005).
[75]P. Boolchand, D. G. Georgiev, and B. Goodman, J. Optoelectron. Adv. Mater. **3**, 703 (2001).
[76]K. Rompicharla, D. I. Novita, P. Chen, P. Boolchand, M. Micoulaut, and W. Huff, J. Phys.: Condens. Matter **20**, 202101 (2008).
[77]N. Toropovs, F. Lo Monte, M. Wyrzykowski, B. Weber, G. Sahmenko, P. Vontobel, R. Felicetti, and P. Lura, Cem. Concr. Res. **68**, 166 (2015).
[78]G. Pickett, Journal Proceedings **38**, 333 (1942).
[79]G. W. Scherer, Transp. Porous Media **110**, 311 (2015).
[80]M. Wyrzykowski and P. Lura, Cem. Concr. Res. **65**, 58 (2014).